Applied Surface Science 268 (2013) 571–578

Contents lists available at SciVerse ScienceDirect

Applied Surface Science

journal homepage: www.elsevier.com/locate/apsusc

Rutile microtubes assembly from nanostructures obtained by ultra-short laser ablation of titanium in liquid

A. De Bonis[a,b,*], A. Galasso[a], N. Ibris[c], A. Laurita[a,c], A. Santagata[b], R. Teghil[a,b]

[a] Dipartimento di Scienze, Università degli Studi della Basilicata, Viale dell'Ateneo Lucano, 10-85100 Potenza, Italy
[b] CNR-IMIP, U.O.S. di Potenza, Zona Industriale di Tito Scalo, 85050 Tito Scalo (PZ), Italy
[c] C.I.G.A.S., Università della Basilicata, Viale dell'Ateneo Lucano, 10-85100 Potenza, Italy

ARTICLE INFO

Article history:
Received 28 October 2012
Received in revised form
18 December 2012
Accepted 6 January 2013
Available online 11 January 2013

Keywords:
Microtubes
Rutile
Ultrashort laser pulses
LAL

ABSTRACT

Pulsed laser ablation of a titanium target in water was performed by an ultra-short laser source (Ti-sapphire, $\lambda = 800$ nm, 1 kHz, 100 fs). The obtained structures were characterized by atomic force microscopy, scanning electron microscopy, X-ray photoelectron spectroscopy, micro-Raman spectroscopy and X-ray diffraction, revealing the presence of non-stoichiometric titanium oxide nanoparticles with a certain amount of crystalline rutile phase. Upon remaining in water the ablated species, the formation of a lamellar phase has been observed. This lamellar phase rolls up to microtubes by remaining in water for a month, through a self-assembling process. The formed microtubes, with an inner diameter of about 2 μm and an outer diameter of 4 μm are characterized by a smooth interior surface and aggregation of nanoparticles on the outer surface.

1. Introduction

Titanium dioxide is a material of large scientific and technological interest due to the wide range of its possible applications ranging from photovoltaic and photocatalyst to photoelectrochromic, sensing, electronics, energy and biotechnology [1–6]. Crystalline TiO_2 exists in three forms: rutile, anatase and brookite. Rutile is the most thermodynamically stable crystalline form, whereas anatase and brookite phases are metastable and transform to rutile when heated. Only anatase and rutile are of practical interest: TiO_2 nanoparticles in the anatase phase are used as photosensitizer and as annihilator for cancerous cells [7]. On the other hand, rutile TiO_2 phase presents some advantages such as higher refractive index, higher dielectric constant and higher chemical stability [8]. The possibility to obtain crystalline TiO_2 in the form of nanoparticles and nanotubes is of particular importance since the higher surface area allows to enhance the titania properties. Moreover, fabrication of nanoscopic and microscopic hollow tubular structures has attracted significant interest owing to their functions in the development of advanced devices [9–12]. Among them, hollow metal oxide microtubes exhibit a range of peculiar properties including a better monodispersity, chemical stability, operability and less obstruction of hollow interior than their nanosized counterparts [13–15]. Due to the lower specific surface area, however, the microtubes usually suffer as compared with the nanotubes in some important special fields, such as catalysis, drug delivery and sensors. Investigations on removing this disadvantage are very important but challenging. In this contest hierarchically structured tubular hollow microtubes have been proposed [16,17]. In fact, such kind of stacking or parallel growth of the building blocks increases further the specific surface area of these microtubes, and hence improves their potential applications in the fields of catalysis, sensors, and drug delivery.

Titanium oxide nanostructures have been grown using various chemical [5] and physical [18] methods such as microemulsion, chemical reduction, hydrothermal chemical process, reverse micelle and pulsed laser ablation (PLA). Otherwise, in the strategies to prepare the microtubes, template-assisted technique is the more feasible and effective way [16]. To date, various templates, including artificial and natural species, have been explored. Liu's group synthesized TiO_2 microtubes by using rod-shaped calcite as template [19]. Additionally, the fabrication of titania microtubes with the porous walls by the replication of human hair has been reported [20]. Motojima et al. described the novel TiO_2 hollow microcoils obtained via carbon microcoils as templates [21,22]. Very recently, the microtubes with the core/shell structures have been prepared via electrospun fibers as soft templates by Chen et al. [23]. Liu et al. [24] obtained TiO_2 microtubes with high length-diameter ratio by using low-cost glass fibers as templates. Although these tubular

* Corresponding author at: Dipartimento di Scienze, Università degli Studi della Basilicata, Viale dell'Ateneo Lucano, 10-85100 Potenza, Italy. Tel.: +39 0971 206249.
E-mail address: angela.debonis@unibas.it (A. De Bonis).

0169-4332/$ – see front matter © 2013 Elsevier B.V. All rights reserved.
http://dx.doi.org/10.1016/j.apsusc.2013.01.015

structures are successfully obtained, these templates are either unusual or difficult to be prepared.

With respect to chemical methods, PLA performed in vacuum or in presence of a buffer gas, is a clean and one step method widely used to obtain thin nanostructured films of borides, carbides and oxides of metals [25–27]. When a pulsed laser source irradiates a target, a local plasma will be produced with electron density, temperature, pressure, composition and species dynamics that are strictly related to the laser pulse duration [28]. Although the ultrashort PLA mechanism is still a matter of debate, nevertheless, it is widely accepted that a femtosecond laser pulse duration is shorter than the full ablation process. This involves, first, the excitation of material thin layer electrons by laser photon absorption, then material lattice relaxation by electron-phonon coupling, and finally the plasma formation. Thus, unlike the nanosecond pulse induced process, the ablated species formed by femtosecond laser pulses do not interact with the laser pulse itself [28,29].

In the last decade, PLA performed in a liquid medium (LAL) has attracted the attention of the scientific community due to the possibility of easily producing extreme synthesis conditions and so obtain novel nanostructures. In LAL process, the laser induced plasma is generated at the liquid–solid interface when the pulsed laser ablate the target. After that, the generated plasma plume will form a dense region in the vicinity of the solid–liquid interface. Since the expansion of the plasma confined in the liquid layer will be delayed, the induced pressure of plasma inside would be greater than that in gaseous or vacuum regimes at the same laser power conditions. The plasma plume formed by laser ablation in liquid media can reach high temperature (4000–6000 K) and high pressure (in the range of 10 GPa) [30]. The species present in a supersaturated plasma interact with each other in a process of nucleation and growth of the nuclei. During this process of growth where the free atoms condense on nuclei, the same nuclei can coalesce together originating the typical polycrystalline structure. Throughout the expansion of the plasma in the liquid buffer, several target and liquid excited or ionized species can participate in chemical reactions at high temperature and pressure conditions. Finally, the rapid quenching of the plasma plume even in an out-of-equilibrium process allows the formation of metastable phases. Indeed, some metastable structures can be frozen due to the rapid cooling down of the laser induced plasma by the confining liquid [31,32]. The experimental differences occurring when PLAs are performed by nanosecond or femtosecond pulses, in both vacuum or gas environments, suggest that, even when a PLA process is carried out in a liquid, the use of femtosecond laser pulses might offer different results than the ones obtainable by longer pulse durations.

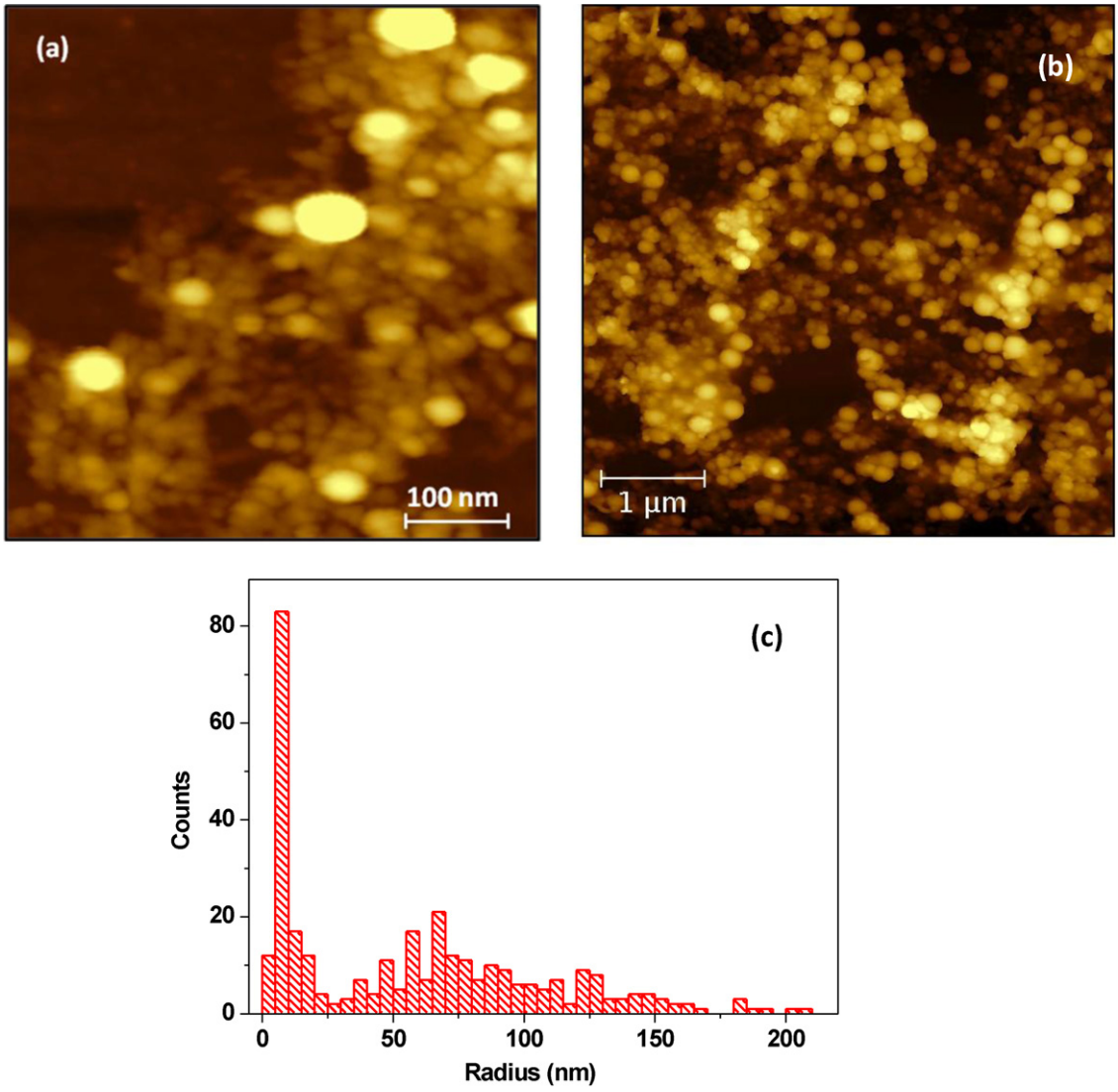

Fig. 1. (a and b)AFM images of the colloidal solution deposited onto a (1 0 0) silicon substrate 5 h after the ablation. (c) Size distribution of the titanium oxide nanoparticles obtained by several AFM images.

Indeed, *T* and *P* evaluated during femtosecond laser ablations can be 2–4-fold higher than those due to nanosecond laser pulses, so new opportunities can be offered by PLA performed in liquid when an ultra-short laser pulse is employed [32–34]. Although the use of laser with a pulse duration in the order of few ps seems to be the optimal condition in terms of efficiency for the production of gold nanoparticles by LAL experiments [35], some evidences have been reported showing that laser ablation in liquid with ultrashort laser sources enable the formation of nanocrystalline metastable phases of different systems [31,36].

There are several reports on synthesis of titanium oxide nanoparticles by PLA in liquid media, carried out by a nanosecond laser source and varying fluence, liquid medium and focusing conditions [7,8,37–40]. In any case the obtained titanium oxide nanoparticles are non-stoichiometric showing different amount of Ti^{2+}, Ti^{3+} and Ti^{4+} due to the non-equilibrium growth conditions. The reported nanoparticles can present different amount of two of the crystalline phases of titanium oxide, in particular Nath et al., showed that using different focusing conditions is possible to enhance the formation of rutile with respect to the anatase phase [7]. Moreover, the dimensions and the aggregation of the nanoparticles can be controlled varying the laser fluence [38]. Titanium monoxide in the disordered cubic phase has been obtained by Semaltianos et al. during the ablation of a metallic titanium target submerged in water by a laser source with a pulse duration of 10.4 ps [39]. The low temperature synthesis employed by this approach is particularly attractive for preparing nanocrystalline TiO_2 having high surface area with no need for a subsequent high temperature treatment. In this work we present the outcomes following the ablation of a titanium target in water performed with a femtosecond laser source. In this case it has been observed the presence in the colloidal solution of non-stoichiometric titanium oxide nanoparticles and nanostructures such as nanowires. The nanoparticles exhibit a certain amount of crystalline rutile phase, whereas no other crystalline phases have been recognized. The evidence of nanostructured titanium oxide microtubes formation driven by ultra-short pulsed laser ablation of a titanium target submerged in water is presented.

2. Experimental methods

Laser ablation was performed by an ultra-short Ti:Sapphire pulsed laser source (Spectra Physics Spitfire Pro XP, 800 nm, 2.7 mJ, 100 fs) with a repetition rates of 1 kHz. The ablation time was 5 min, corresponding to 300,000 laser shots. The laser beam was focused perpendicularly to the surface of a metal plate of titanium by a 5 cm plano-convex focal length lens. The laser spot area on the solid target was 1×10^{-3} cm^2 and the laser energy reaching the target surface was 2 mJ for a fluence of 2 J/cm^2. The solid sample, covered by a 1 cm bidistilled deionized milli-Q water column, was contained in a standard spectroscopic UV quartz cuvette (3.5 ml). A micrometer translation stage was employed in order to minimize crater formation on the solid sample surface due to successive laser beam pulses. The obtained solution was maintained at room temperature for 1 month, without any other treatment. After this period of time a bundle of fibers was observed in the solution.

The nanoparticles and bundles recovered from such samples were deposited onto a monocrystalline polished silicon (1 0 0) surface to perform the AFM, SEM, micro-Raman, XPS and XRD measurements. A Park XE-120 Atomic Force Microscope fully equipped for surface analysis was used for imaging the samples topography. Surface images were acquired in tapping mode using commercial, unmodified diamond tips. All AFM measurements were performed in air on duplicate samples. To limit the risk of the probed surface morphology being affected by possible random local effects and to increase the representativeness of the whole surface, three regions of the surface were scanned for each sample using different scan size areas.

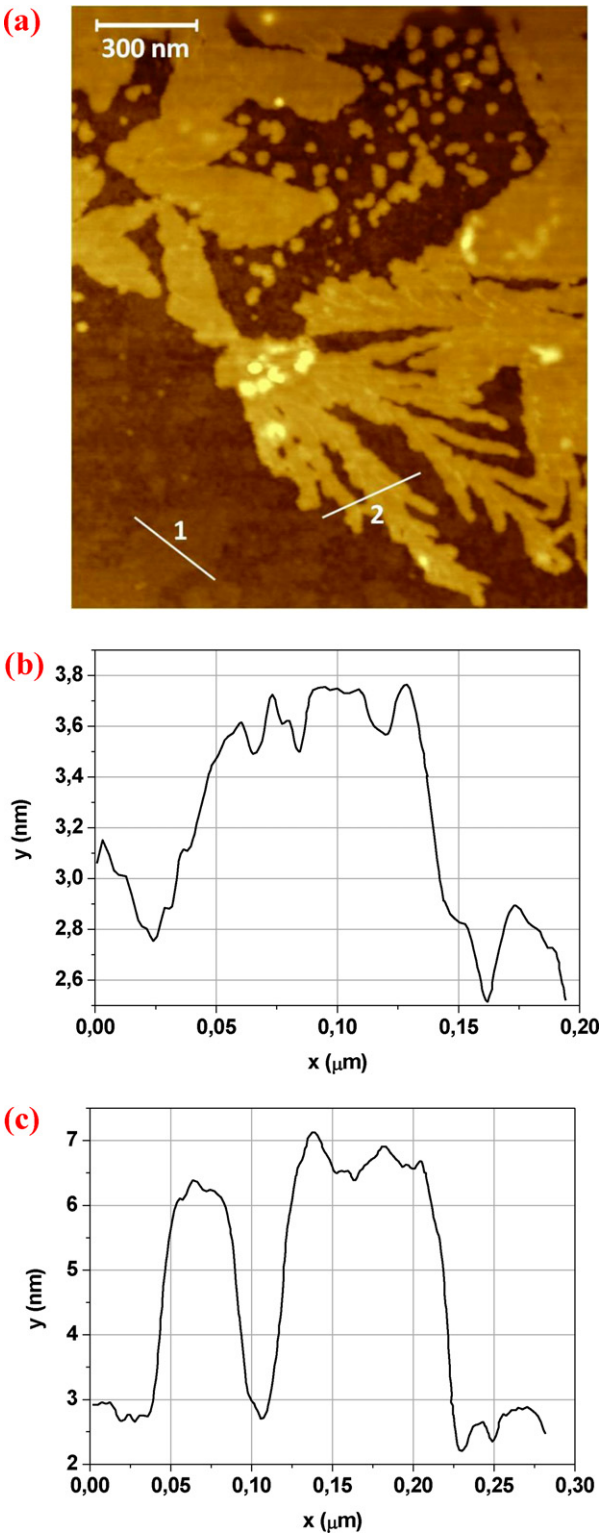

Fig. 2. (a) AFM image of the colloidal solution deposited onto a (1 0 0) silicon substrate few hours after the ablation. The lamellar phase is evidenced; (b) height profile of line 1; (c) height profile of line 2.

The SEM images were obtained by a Philips-Fei ESEM XL30-LaB6 after coating each sample by a sputtered Au thin layer (ca. 10 nm).

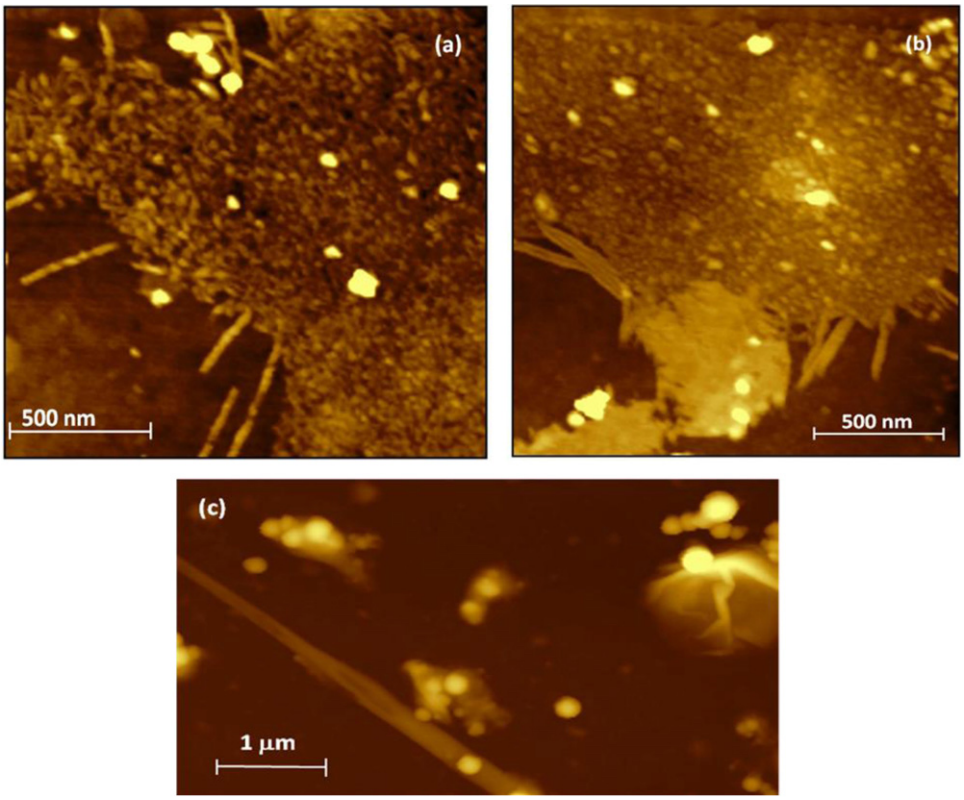

Fig. 3. (a and b) AFM image of the colloidal solution deposited onto a (1 0 0) silicon substrate two days after the ablation. (c) AFM image of the colloidal solution deposited onto a (1 0 0) silicon substrate eight days after the ablation.

XPS spectra were acquired by a LH Leybold X1 spectrometer using non-monochromatized MgKα radiation operating at a constant power of 260 W. Wide and detailed spectra were collected in Fixed Analyzer Transmission (FAT) mode with a pass energy of 50 eV and channel widths of 1.0 and 0.1 eV, respectively. The acquired XPS spectra were analyzed using a curve-fitting program, Googly, described by Castle and Salvi [41], which allows the simultaneous fitting of photo-peaks in the form of a Voigt function and their associated background in a wide energy range.

Raman spectra were acquired by a micro-Raman Jobin Yvon (LABRAM HR800) in backscattered configuration equipped with two gratings (600 and 1800 grooves/mm) and an optical Olympus microscope having 10×, 50×, and 100× objectives. The spectrometer was connected to a Peltier cooled CCD detector. The excitation was obtained by using a HeNe laser source (λ = 632.8 nm). The laser power was maintained at 10 mW, whereas the spectra were acquired using the 1800 grooves/mm grating and the 100× objective. In this condition, the estimated spectrum resolution was about 1 cm^{-1}.

XRD analysis were performed by a D-max-Rapid Rigaku microdiffractometer with a CuK_α radiation, equipped with a curved-image-plate detector, a flat graphite monochromator, a variety of beam collimators, a motorized stage and a microscope for accurate positioning of the sample. The data were collected in reflection mode using 0.3 mm collimator and a collection time of 10 min.

3. Results and discussion

3.1. Morphological and structural characterization

AFM analysis for the representative deposits retrieved from titanium colloidal solution 5 h after the laser ablation and the corresponding nanoparticles size distribution are reported in Fig. 1a, b and c, respectively. AFM images were taken in several regions of the deposit. The nanoparticles size distribution shows that the deposit consists of nanoparticles with radius from 5 to about 200 nm with the 50% of the nanoparticles having radius up to 50 nm. The average particle size is 57 nm and the shape of the particles, assembled in a closely packed manner or as nano-chain aggregate, as reported in Fig. 1b, is almost perfectly spherical, indicating that the growth process does not occur along a preferred direction. Moreover, in Fig. 2a is reported an AFM image, obtained onto a different region of the same deposit, where, it is shown, together with nanoparticles, the presence of a lamellar phase with a thickness ranging from 1.5 to 3 nm. Maintaining the colloidal titanium solution in water for two days, both the lamellar phase and the close packed nanoparticles give rise to nanowiskers as is reported Fig. 3a. These nanostructures, with a diameter and thickness of tens and few nanometers, respectively, seem to be originated from the coalescence of nanoparticles or rolling up of the lamellar phase. These nanostructures develop directly in water. In fact, eight days after laser ablation, it is possible to observe the presence of bigger structures, characterized by a flat outer surface and with a diameter and thickness of hundreds and tens of nanometer, respectively (Fig. 3c). After remaining four weeks in water, additional tubular materials were observed in the colloidal solution. SEM images of this material, repetitively rinsed with distilled water and soaked in an ultrasonic bath for 30′, are presented in Fig. 4a–b. Fig. 4a gives an overview of the microtubes at low magnification. These tubular material, that could be assembled from highly activated nanocondensates, has a mean diameter as large as 4 μm and were entangled and bifurcated at triple junction. In Fig. 4b the inner flat surface of a truncated microtube, with an internal diameter of 2 μm, is reported. Moreover, on the external microtubes surface the coalescence of nanoparticles gives rise to the development of rigid walls about 1 μm thick. The resulting external diameter of microtubes is about 4 μm (Fig. 5).

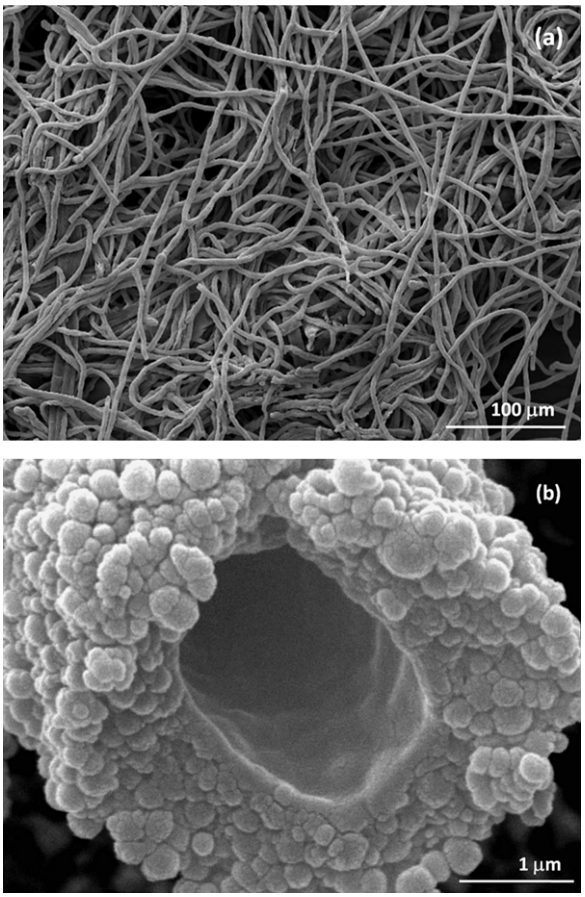

Fig. 4. SEM image of titanium oxide microtubes at low (a) and higher (b) magnification.

Nanoparticles and microtubes deposited onto monocrystalline silicon substrate were characterized by XRD and micro-Raman analysis. In Fig. 6 micro-XRD spectra of nanoparticles and microtubes are reported. In both samples, Si (1 0 0) Bragg peaks are dominant and thin films contribute with weaker signals. Beside Si (1 0 0) signals three peaks at 36.1°, 41.3° and 54.4° are present. These peaks are indexed as (1 0 1), (1 1 1) and (2 1 1) planes of TiO_2 crystal in the form of tetragonal rutile structure, respectively,

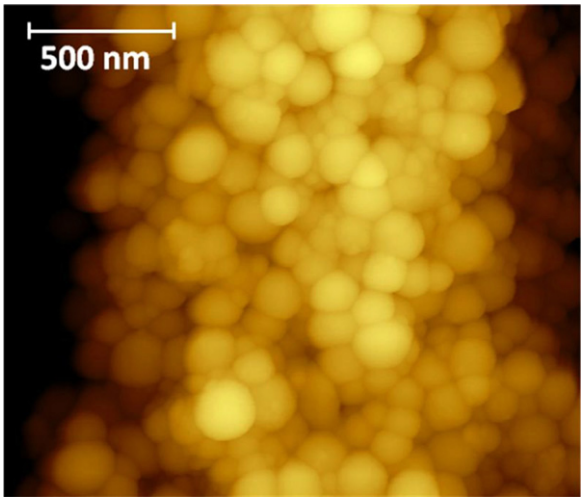

Fig. 5. AFM image of the outer surface of a titanium oxide microtube.

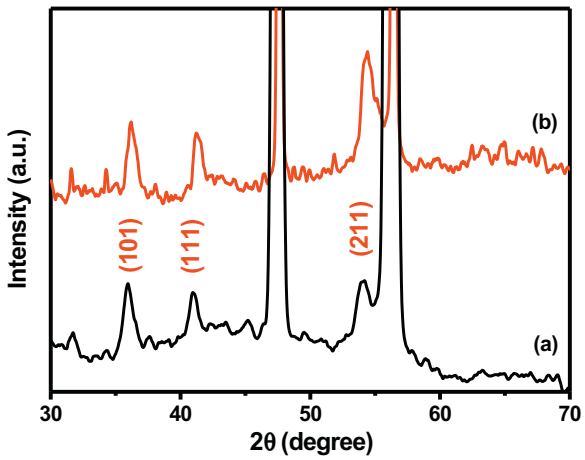

Fig. 6. XRD spectra of (a) nanoparticles and (b) microtubes deposited onto a silicon (1 0 0) substrate.

in agreement with standard diffraction data of rutile TiO_2 (JCPDS file no. 87-0710). The broad feature of the rutile peaks observed in the spectra may arise from the presence of crystallite of very small diameter. From the Debye–Scherrer formula, the peak at 36.1° provides with crystallites size of 12 nm. The findings of XRD analysis are confirmed by micro-Raman measurements. In Fig. 7 the Raman scattering spectra of nanoparticles and microtubes are presented. Both structures display a characteristic TiO_2 rutile spectrum, with signals at 260, 426 and 608 cm^{-1}, assigned to a second order phonon, and to E_g and A_{1g} modes of TiO_6 octrahedra in the rutile arrangement, respectively [42]. The broad band centered at 710 cm^{-1}, assigned to a TiOH vibrational mode, suggests the presence of hydroxyl groups [43]. The observed shift and broadening of peaks reported in these spectra with respect to Raman signature of crystalline rutile can be ascribed to phonon confinement and to a certain distortion of the TiO_6 octahedra [37], which can be due to the presence of some amorphous phase. Although the size and morphology occurring differences, there are no significant changes in Raman shifts between microtubes and nanoparticles. It should be pointed out that the observed Raman spectra of microtubes are significantly different from those of hydrogen titanate $H_2Ti_3O_7$ [42], that represents the main component of TiO_2 nanotubes produced by hydrothermal treatment of titania with NaOH. This finding suggests that a strongly different process occurs by

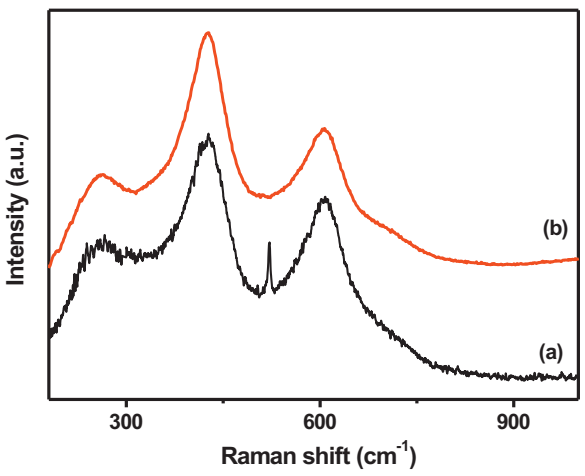

Fig. 7. Raman spectra of (a) nanoparticles and (b) microtubes deposited onto a silicon (1 0 0) substrate.

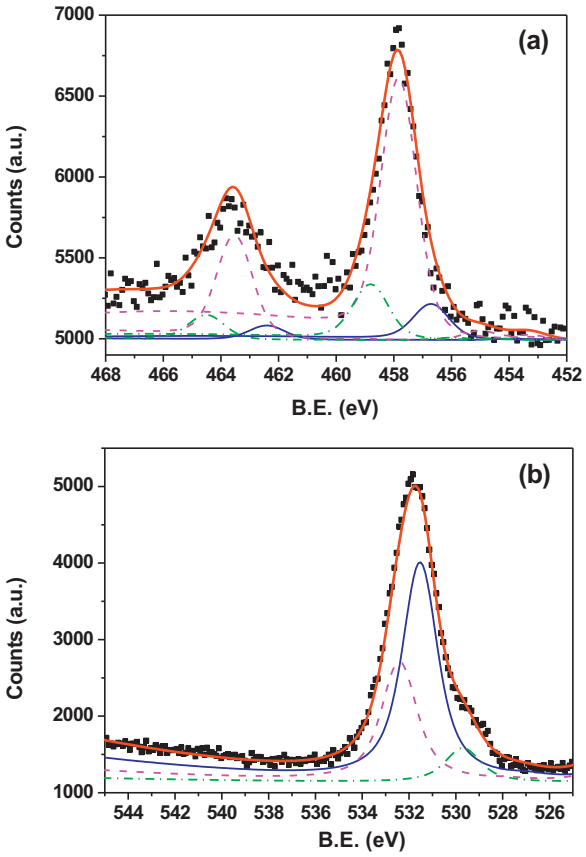

Fig. 8. XPS spectra of titanium oxide nanoparticles deposited onto a silicon (1 0 0) substrate. (a) Ti 2p region. Solid line (-) $Ti2p_{3/2}$ and $Ti2p_{1/2}$ of Ti_2O_3, dash-dot line (-.-)$Ti2p_{3/2}$ and $Ti2p_{1/2}$ of TiO_2, dashed line (—)$Ti2p_{3/2}$ and $Ti2p_{1/2}$ of TiOH. (b) O1s region. Solid line (-) O1s of Ti_2O_3, dash-dot line (-.-) O1s of TiO_2, dashed line (—) O1s of TiOH.

water driven growth of microtubes obtained in this work from the other titanate nanotubes reported in literature.

3.2. XPS analysis

In Fig. 8a–b are reported the XPS spectra of the titanium oxide nanoparticles: the sub-bands analysis of the Ti 2p and O 1s core level spectra of the sample are also shown. The Ti 2p signal, characterized by spin orbit (1/2, 3/2) Ti doublet components, can be decomposed into three contributions corresponding to three different titanium species. Voigt shape functions, with the same FWHM for each peak were used for the deconvolution. The ratio area of the doublets is equal to 0.5 and the binding energy difference is 5.7 eV, in agreement with literature data [8]. The three Ti $2p_{3/2}$ peaks, located at BE 456.7, 457.8 and 458.8 eV are assigned to in Ti_2O_3, Ti—OH and TiO_2, respectively. The O 1s region can be decomposed with three contributions at about 529.7, 531.5 and 532.4 eV, assigned at O—Ti^{4+}, O—Ti^{3+} and HO—Ti, respectively [44]. The contribution of organic contaminants such as C—O and O—C=O, always present, cannot be distinguished from the hydroxyl groups and Ti_2O_3 signals since they have similar binding energies [41]. From XPS analysis is evident that suboxide phases are significantly present in the rutile nanoparticles. Moreover, the partially oxidized Ti surface shows a high reactivity toward OH groups. In fact, the hydroxyl groups were likely associated with surface sites of nonstoichiometric titania nanoparticles. It is noteworthy to stress that not any significant difference has been evidenced in XPS spectra between microtubes and nanoparticles. The aggregation of nanoparticles on the external surface of microtubes justify it.

4. Discussion

Immediately after an ultra-short laser pulse hits a titanium target submerged in water manifold process are going to be involved. First of all, the laser induces a high temperature and a high pressure Ti plasma, which interact with the surrounding liquid medium. At the plasma–liquid interface an ultrafast quenching of the Ti plasma is caused. The consequent dense cloud of titanium species so generated leads to the formation of embryonic Ti clusters. At the same time the laser–water interactions may cause photodissociation of the water due to one-photon or multiple-photon excitation and the formation of bubbles at the laser spot [45]. It should be also considered that during the interaction at Ti plasma–liquid interface, the surrounding solvent can be excited, ionized and dissociated. The layer of vapor produced around the laser induced plasma could grow into a cavitation bubble which expand and then collapse, on a time scale on the order of hundreds of microseconds. Water vapor, ionized and excited atomic and molecular hydrogen and oxygen so formed give rise to a high reactive “water plasma” inside the cavitation bubble. The interactions among the water plasma and the formed active metallic clusters provide, through chemical reactions, the oxidation of metallic Ti and final formation of Ti_xO_y nanostructures. Soluble oxygen in water or products of photodissociation may aid the nanoparticles oxidation [8,33,37]. It has been reported that the ablation of active metals such as titanium in water, gives as primary products its hydroxides. These hydroxide seeds can either become dehydrated into oxide by water loss, or become clustered to form hydroxide nanoparticles [46]. As a consequence of the process complexity different kinds of titanium oxide and hydroxide nanostructures can be grown. The nanoparticles growth process takes place inside the cavitation bubble. So, when the bubble reaches its maximum radius and the gas inside the bubble is in equilibrium with the surrounding liquid, the newly formed nanoparticles undergo a rapid cooling from plume temperature to the temperature of the solvent. In this experimental conditions the formation of high temperature stable phase (rutile) is possible together with the presence of titanate amorphous phase due to the shock-wave loading induced by the pulsed laser ablation in liquid process itself [32]. Moreover, the preferential condensation and nucleation of vaporized plume species on the interfaces between water and gas bubble, in order to minimize the interfacial surface free energy, can be argued [39]. The AFM images (Fig. 1a and b) and structural characterizations here reported have shown that during ultra-short laser ablation of titanium in water about 50 nm radius nanoparticles have been formed. These can be indeed caused by the presence of very small rutile crystallite in the amorphous matrix. Considering the XPS and Raman data, it can be stated that these colloids are hydroxylated via adsorbed hydroxyl moieties. This reaction could be favored on the Ti^{3+} sites [44]. The co-presence of Ti_2O_3, TiO_2 and TiOH, detected by XPS, denotes the occurrence of nonstoichiometric titania phases and hence titanium and/or oxygen vacancies. The hydroxyl groups can be related to different nonstoichiometric sites of the titania surface inducing interactions, such as hydrogen bonds, with the surrounding water molecules [37]. Huang et al. [37] have also shown that a high amount of hydroxyl groups were present in titania microtubes formed during laser ablation in water by using a nanosecond laser source and that their protonated structure was different from that of titanium hydrate such as $H_2Ti_3O_7$ [47,48]. Stress strain of amorphous titania has been considered, by scrolling up of its lamellae forms, as the leading factor for the amorphous microtubes formation observed by Huang et al. [37]. The presence of Ti^{3+} and Ti^{4+} oxidation state justifies that interstitial protons H^+ can act as charge compensating of cation vacancies. The presence of H^+ into the amorphous titania plate interlayer space can be relevant for inducing a strain field between the surface layer of the

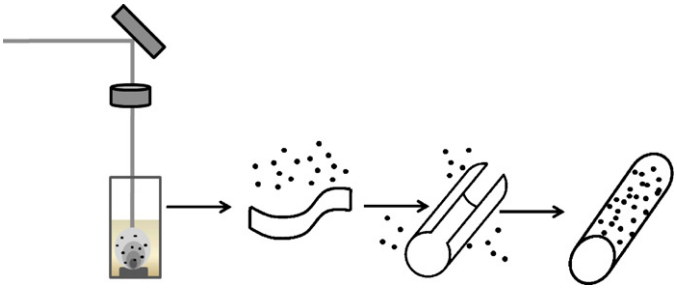

Fig. 9. Schematic illustration for the proposed formation process of titania microtubes.

amorphous lamellae when hydrogen deficiency may be induced on it. Hydroxyl groups present at the titania plate surface can form H_2O by reacting with the surface H^+ ions so that Ti—O bonds undergo a contraction [47]. This process can lead to titania outer monolayer stress strain causing its peeling-off from the remaining amorphous plate and then scrolling-up into nanotubes. Such a mechanism has been considered also for explaining the formation of TiO_2 based nanotubes when a crystalline TiO_2 powder reacts with a NaOH solution [42,47]. In this particular experimental conditions nanotubes present the well known structure of titanium hydrate $H_2Ti_3O_7$. The dimension of such nanotubes is controlled by this surface tension together with interlayer coupling energy and Coulomb force [42,47]. On the contrary, in this work, the presence of OH^- species due to the interaction of the water solvent with a high energetic laser source and with a plume characterized by extreme value of temperature, could induce the delamination of the amorphous fraction of the titania nanostructures formed during the laser ablation. Indeed, this can lead to the observed formation of nonstoichiometric TiO_2 based nanoparticles first and then by dwelling in water the ablated Ti species, the successive growth of needle-shaped products, nanotubes and the observed microtubes. For the existence of needle-shaped products and nanotubes titania plates or lamellae formations are needed [42,47]. As it has been reported, these have been indeed observed in the AFM image presented in Fig. 2a and probably even stabilized via oxolation during the laser ablation process. Afterwards, upon ripening in water, they first evolve into nanowiskers and then to belts of some hundreds of nanometers large. Finally, leaving the formed species in water for one month, it has been evidenced the formation of microtubes with an internal smooth surface and an external surface formed by the aggregation and coalescence of nanoparticles. In Fig. 9 a schematic illustration of the proposed process of titania microtubes is reported. We believe that the origin of the microtubes is related to the initial lamellar phase reported in this work. Conversely, the formation of microtubes directly from nanoparticles aggregation has been observed, as it is reported in literature [19–24], but only in presence of templates such as glass fibers or rod-shaped calcite. With regard to the observed agglomerate structures it can be considerd that the detected Ti—OH species can definitely play a relevant role in hydrogen bond formation and the nanoparticles aggregation and coalescence onto the microtubes external surface.

5. Conclusions

Laser ablation of a titanium target submerged in water, by using a high power density configuration (2×10^{16} W/cm^2) induces the formation of titania nanoparticles with a certain quantity of rutile phase. A XPS analysis has shown the co-presence of Ti_2O_3, TiO_2 and TiOH, denoting the occurrence of nonstoichiometric titania phases and hence cation and/or oxygen vacancies. Upon remaining in water the ablated species it has been obsreved the formation of lamellar nanostructures. These evolve initially into nanowiskers, then to nanobelts and finally into microtubes. The presence of OH— species could induce the delamination of the titania nanostructures and the occurrence of Ti^{3+} and Ti^{4+} oxidation states can justify that interstitial protons H^+ can lead toward a strain field between the surface layers inducing their peeling-off and formation of microtubes by a self-assembling mechanism. The detected Ti—OH species can indeed play a relevant role in aggregation and coalescence of nanoparticles on the observed outer surface of the microtubes by hydrogen bonds formation, opening a new root for preparing the TiO_2 microtubes by the ultra-short LAL method.

Acknowledgments

This paper draws on work undertaken as part of the project CLAN (Combined Laser Nanotechnology) co-financed by the Operational Programme ERDF Basilicata 2007–2013.

The authors express their gratefulness to Dr. L. Medici (CNR-IMAA- Tito Scalo–PZ–Italy) for performing XRD analysis.

References

[1] M. Gratzel, Nature 414 (2001) 338–344.
[2] Y. Ohko, T. Tatsuma, T. Fujii, K. Naoi, C. Niwa, Y. Kubata, A. Fujishima, Nature Materials 2 (2003) 29.
[3] M.C. Carotta, M. Ferroni, D. Gnani, V. Guidi, M. Merli, G. Martinelli, M.C. Casale, M. Notaro, Sensors and Actuators B 58 (1999) 310–317.
[4] X. Gao, H. Zhu, G. Pan, S. Ye, Y. Lan, F. Wu, D. Song, Journal of Physical Chemistry B 108 (2004) 2868.
[5] X. Chen, S.S. Mao, Chemical Reviews 107 (2007) 2891–2959.
[6] U. Diebold, Surface Science Reports 48 (2003) 53–229.
[7] A. Nath, S.S. Laha, A. Khare, Applied Surface Science 257 (2011) 3118–3122.
[8] P. Liu, W. Cai, L. Wan, M. Shi, X. Luo, W. Jing, Transactions of Nonferrous Metals Society of China 19 (2009) s74–s747.
[9] Y. Xia, P. Yang, Y. Sun, Y. Wu, B. Mayers, B. Gates, Y. Yin, F. Kim, H. Yan, Advanced Materials 15 (2003) 353–389.
[10] L. Qian, Z.S. Jin, S.Y. Yang, Z.L. Du, X.R. Xu, Chemistry of Materials 17 (2005) 5334–5338.
[11] F.Z. Song, X.Q. Shen, J. Xiang, Y.W. Zhu, Journal of Alloys and Compounds 507 (2010) 297–301.
[12] M. Paulose, O.K. Varghese, G.K. Mor, C.A. Grimes, K.G. Ong, Nanotechnology 17 (2006) 398–402.
[13] B. Liu, S. Wei, Y. Xing, D. Liu, Z. Shi, X. Liu, X. Sun, S. Hou, Z. Su, Chemistry - A European Journal 16 (2010) 6625–6631.
[14] K. Dietrich, C. Strelow, C. Schliehe, C. Heyn, A. Stemmann, S. Schwaiger, S. Mendach, A. Mews, H. Weller, D. Heitmann, T. Kipp, Nano Letters 10 (2010) 627–631.
[15] K. Kumar, B. Nandan, V. Luchnikov, E.B. Gowd, M. Stamm, Langmuir 25 (2009) 7667–7674.
[16] R. Chen, M. Wang, Materials Letters 69 (2012) 41–44.
[17] G. Tian, Y. Chen, W. Zhou, K. Pan, C. Tian, X. Huang, H. Fu, CrystEngComm 13 (2011) 2994–3000.
[18] M. Fusi, E. Maccallini, T. Caruso, C.S. Casari, A. Li Bassi, C.E. Bottani, P. Rudolf, K.C. Prince, R.G. Agostino, Surface Science 605 (2011) 333–340.
[19] D. Liu, M. Yates, Langmuir 23 (2007) 10333–10341.
[20] S. Liu, J. He, Journal of the American Ceramic Society 88 (2005) 3513–3514.
[21] S. Motojima, T. Suzuki, Y. Noda, A. Hiraga, H. Iwanaga, T. Hashishin, Y. Hishikawa, S. Yang, X. Chen, Chemical Physics Letters 378 (2003) 111–116.
[22] S. Motjima, T. Suzuki, Y. Noda, A. Hiraga, S. Yang, X. Chen, T. Hashishin, Y. Hishikawa, Journal of Materials Science 39 (2004) 2663–2674.
[23] H. Chen, N. Wang, J. Di, Y. Zhao, Y. Song, L. Jiang, Langmuir 26 (2010) 11291–11296.
[24] W. Liu, L. Zhang, L.X. Cao, G. Su, Y.G. Wang, Journal of Alloys and Compounds 509 (2011) 3419–3424.
[25] R. Teghil, L. D'Alessio, A. De Bonis, A. Galasso, N. Ibris, A.M. Salvi, A. Santagata, P. Villani, Journal of Physical Chemistry A 113 (2009) 14696–14974.
[26] J.V. Rau, A. Latini, R. Teghil, A. De Bonis, M. Fosca, R. Caminiti, V. Rossi Albertini, ACS Applied Materials and Interfaces 3 (2011) 3738–3743.
[27] R. Teghil, A. De Bonis, A. Galasso, P. Villani, A. Santagata, Applied Surface Science 254 (2007) 1220–1223.
[28] O. Albert, S. Roger, Y. Glinec, J.C. Loulergue, J. Etchepare, C. Boulmer-Leborgne, J. Perriere, E. Millon, Applied Physics A 76 (2003) 319–323.
[29] A. De Bonis, A. Galasso, V. Marotta, S. Orlando, A. Santagata, R. Teghil, S. Veronesi, P. Villani, A. Giardini, Applied Surface Science 252 (2006) 4632–4636.
[30] A. De Giacomo, A. De Bonis, M. Dell'Aglio, O. De Pascale, R. Gaudiuso, S. Orlando, A. Santagata, G.S. Senesi, F. Taccogna, R. Teghil, Journal of Physical Chemistry C 115 (2011) 5123–5130.
[31] A. Santagata, A. De Bonis, A. De Giacomo, M. Dell'aglio, A. Laurita, G.S. Senesi, R. Gaudiuso, S. Orlando, R. Teghil, G.P. Parisi, Journal of Physical Chemistry C 115 (2011) 5160–5164.
[32] G.W. Yang, Progress in Materials Science 52 (2007) 648–698.

[33] V. Amendola, M. Meneghetti, Physical Chemistry Chemical Physics 11 (2009) 3805–3821.
[34] P. Liu, H. Cui, C.X. Wang, G.W. Yang, Physical Chemistry Chemical Physics 12 (2010) 3942–3952.
[35] D. Riabinina, M. Chaker, J. Margot, Nanotechnology 23 (2012), 135603 (4 pp.).
[36] D. Tan, G. Lin, Y. Liu, Y. Teng, Y. Zhuang, B. Zhu, Q. Zhao, J. Qiu, Journal of Nanoparticle Research 13 (2011) 1183–1190.
[37] C. Huang, J. Bow, Y. Zheng, S. Chen, N. Ho, P. Shen, Nanoscale Research Letters 5 (2010) 972–985.
[38] F. Barreca, N. Acacia, E. Barletta, D. Spataro, G. Currò, F. Neri, Applied Surface Science 256 (2010) 6408–6412.
[39] N.G. Semaltianos, S. Logothetidis, N. Frangis, I. Tsiaoussis, W. Perrie, G. Dearden, K.G. Watkins, Chemical Physics Letters 496 (2010) 113–116.
[40] V. Caratto, M. Ferretti, L. Setti, Applied Surface Science, 258, 2393–2396.
[41] J.E. Castle, A.M. Salvi, Journal of Electron Spectroscopy 114–116 (2001) 1103–1113.
[42] T. Gao, H. Fjellvag, P. Norby, Inorganic Chemistry 48 (2009) 1423–1432.
[43] K.R. Zhu, Y. Yuan, M.S. Zhang, J.M. Hong, Y. Deng, Z. Yin, Solid State Communications 144 (2007) 450–453.
[44] P.M. Kumar, S. Badrinarayanan, M. Sastry, Thin Solid Films 358 (2000) 122–130.
[45] Z. Yan, R. Bao, D.B. Chrisey, Nanotechnology, 21, 145609 (8 pp.).
[46] H. Zeng, X.W. Du, S.C. Singh, S.A. Kulinich, S. Yang, J. He, W. Cai, Advanced Functional Materials 22 (2012) 1333–1353.
[47] S. Zhang, L.M. Peng, Q. Chen, G.H. Du, G. Dawson, W.Z. Zhou, Physical Review Letters 91 (2003) 2561031–2561034.
[48] Q. Chen, W. Zhou, G. Du, L.M. Peng, Advanced Materials 14 (2002) 1208–1211.